

**Technical Report No. 32-214**

# **A Simple Beamshaping Device for Cassegrainian Antennas**

**P. D. Potter**



**JET PROPULSION LABORATORY  
CALIFORNIA INSTITUTE OF TECHNOLOGY  
PASADENA, CALIFORNIA**

**January 31, 1962**

NATIONAL AERONAUTICS AND SPACE ADMINISTRATION  
CONTRACT NO. NAS 7-100

**Technical Report No. 32-214**

**A Simple Beamshaping Device for  
Cassegrainian Antennas**

**P. D. Potter**

A handwritten signature in dark ink, appearing to read "R. Stevens", is written over a horizontal line.

R. Stevens, Chief  
Communications Elements Research

JET PROPULSION LABORATORY  
CALIFORNIA INSTITUTE OF TECHNOLOGY  
PASADENA, CALIFORNIA

January 31, 1962

Copyright© 1962  
Jet Propulsion Laboratory  
California Institute of Technology

## CONTENTS

I. Introduction . . . . .	1
II. Aperture Efficiency and Effective Noise Temperature . . . . .	2
III. The Cassegrainian System . . . . .	6
IV. Beamshaping Modification . . . . .	7
V. Full-Scale Tests . . . . .	10
Acknowledgment . . . . .	12
References . . . . .	13

## FIGURES

1. Paraboloid geometry . . . . .	14
2. Effect of spillover . . . . .	14
3. Cassegrainian system . . . . .	15
4. Conical subreflector approximation . . . . .	15
5. Experimental ring scatterer . . . . .	16
6. Measured scattering pattern of ring . . . . .	17
7. Cassegrainian pattern synthesis . . . . .	18
8. Predicted Cassegrainian pattern . . . . .	18
9. Geometry of shaped-beam subreflector . . . . .	19
10. Scale model feed system and mount . . . . .	20
11. Scale model subreflector . . . . .	20

## FIGURES (Cont'd)

12a.	E-plane pattern of modified reflector, $\theta = 15.4$ deg . . . . .	21
12b.	H-plane pattern of modified reflector, $\theta = 15.4$ deg . . . . .	21
13a.	E-plane pattern of modified reflector, $\theta = 18.4$ deg . . . . .	22
13b.	H-plane pattern of modified reflector, $\theta = 18.4$ deg . . . . .	22
14a.	E-plane pattern of modified reflector, $\theta = 21.4$ deg . . . . .	23
14b.	H-plane pattern of modified reflector, $\theta = 21.4$ deg . . . . .	23
15a.	E-plane pattern of modified reflector, $\theta = 24.4$ deg . . . . .	24
15b.	H-plane pattern of modified reflector, $\theta = 24.4$ deg . . . . .	24
16.	45-deg-plane pattern of modified subreflector, $\theta = 18.4$ deg . . . .	25
17.	Cross-polarized 45-deg-plane pattern of modified subreflector, $\theta = 18.4$ deg . . . . .	26
18.	E-plane pattern of unmodified subreflector . . . . .	27
19.	H-plane pattern of unmodified subreflector . . . . .	28
20.	45-deg-plane pattern of unmodified subreflector . . . . .	29
21.	Cross-polarized 45-deg-plane pattern of unmodified subreflector . .	30
22.	Spillover vs flange angle . . . . .	31
23.	Phase measuring system . . . . .	32
24.	Phase error plot, 45-deg plane, $\theta = 18.4$ deg . . . . .	33
25.	Aperture integration plot, 45-deg plane, $\theta = 18.4$ deg . . . . .	33
26.	Vector integration diagram . . . . .	34
27.	Aperture efficiency vs flange angle . . . . .	35
28.	Full-scale Cassegrainian installation . . . . .	36

FIGURES (Cont'd)

29.	Secondary pattern, E-plane . . . . .	37
30.	Secondary pattern, H-plane . . . . .	38

## ABSTRACT

A simple beamshaping modification for Cassegrainian systems is described. A qualitative analysis is used to describe this device as well as to explain the poor performance observed with an unmodified Cassegrainian system. Experimental data are presented on both the modified and unmodified systems. The modification reduces spillover by a factor of 2 to a value of only 1.3%. Simultaneously, the aperture efficiency is increased from 50% for the unmodified system to 60% for the modified system. Field measurements on an 85-ft modified Cassegrainian system are described which experimentally verify the applicability of the modified subreflector to low-noise antenna design. The measured zenith antenna temperature for this system is 9.5° K; measured aperture efficiency is 50%.

## I. INTRODUCTION

The use of paraboloidal reflectors for large-aperture ground-based antennas is widespread. At the present time, this type of antenna appears to be unrivaled in the low noise application as a good compromise between performance and cost.

The design and construction of a large ground antenna is a difficult financial, structural, and servomechanical task. When the task is undertaken it is imperative that the maximum RF performance be achieved. Although this problem has only recently interested the antenna design community, the theoretical possibility of achieving extremely high aperture efficiency (on the order of 90%), while at the same time achieving very low spillover (on the order of 1 - 2%) certainly exists. For this application, the ordinary horn-type antenna is only a zero-order solution to the paraboloid feed problem. The antenna designer's difficulty in simultaneously obtaining uniform aperture illumination and low spillover is virtually unknown to the optical telescope designer. It is natural, therefore, to attempt to apply optical design approaches to ground antennas which are extremely large compared to the operating wavelength. The two-reflector Cassegrainian system is a popular example of such an attempt. One of the most attractive features of this system is that the feedhorn, microwave circuitry, and receiving equipment are mounted near the surface of the paraboloid, rather than near its focus. This approach has obvious operational advantages, particularly with very large antennas. Such a simple thing as the ready adaptability of air conditioning to a maser, follow-on amplifier, and their

instrumentation may be a significant factor in system performance. Thus for practical reasons alone, it may be desirable to use the Cassegrainian feed system.

From the performance standpoint, however, an optically designed system leaves much to be desired. Even for antennas which are hundreds of wavelengths in diameter the spillover properties of the Cassegrainian feed system are not exceptionally good. This fact is illustrated herein with typical experimental data. A simple analysis is advanced which semiquantitatively predicts the performance of an unmodified Cassegrainian feed system in terms of its size in wavelengths. Correlation with experimental data is shown.

Based on the theory advanced in this report, a simple beamshaping device was developed (Ref. 1) which drastically improves the spillover performance and, to some extent, the aperture efficiency. Complete experimental data are presented.

## II. APERTURE EFFICIENCY AND EFFECTIVE NOISE TEMPERATURE

Generally, the most important performance parameters associated with large ground-based paraboloids are the aperture efficiency and the noise temperature. Calculation of aperture efficiency of a paraboloidal antenna amounts to a calculation of the radiated axial far field strength for a given power input. As pointed out by Silver (Ref. 2), the result of such an axial field strength calculation is independent of whether the aperture field or the surface current method of calculation is used. It turns out, in fact, that the calculation is generally more expeditiously performed as an integration of a current on the reflector

surface. Using this method, it can be shown (Ref. 3) that for a uniformly phased paraboloid illumination the aperture efficiency  $\eta$  is given by:

$$\eta = \frac{1}{4\pi^2} \cot^2\left(\frac{\Psi}{2}\right) G_{\text{of}} \left| \int_0^{2\pi} \int_0^{\Psi} E_f(\psi, \xi) \tan\left(\frac{\psi}{2}\right) d\psi d\xi \right|^2 \quad (1)$$

where

$\Psi$  = aperture half angle

$\xi, \psi$  = angular coordinates of a point on the reflector surface

$G_{\text{of}}$  = feed system power gain

$E_f(\psi, \xi)$  = normalized field system voltage radiation pattern

The geometry used in Eq. (1) is shown in Fig. 1. The maximum feed gain  $G_{\text{of}}$  and the radiation pattern  $E_f(\psi, \xi)$  are, of course, readily measurable quantities for any given feed system. In practice,  $E_f(\psi, \xi)$  may be established by measuring radiation patterns as a function of  $\psi$  for two or more discrete values of  $\xi$ . In this case, (1) reduces to (Ref. 3):

$$\eta \approx \cot^2\left(\frac{\Psi}{2}\right) G_{\text{of}} \left| \frac{1}{N} \sum_{n=1}^{n=N} \int_0^{\Psi} E_f(\psi, \xi_n) \tan\left(\frac{\psi}{2}\right) d\psi \right|^2 \quad (2)$$

The error introduced by this sampling process in  $\xi$  is discussed in Ref. 3 and is generally very small. It should be noted that (2) takes account of several significant factors which are generally neglected by the aperture integration method (Ref. 2); mismatch losses, dissipative feed losses and cross-polarization losses are all included in the experimental determination of  $G_{\text{of}}$  and  $E_f(\psi, \xi_n)$ . A

weighted graph paper may be constructed (Ref. 3) which permits simple but accurate graphical evaluation of (2).

The recent advent of maser and parametric devices in communication systems has reduced receiver system noise levels to the point where the antenna itself can be a serious contributor. Although the noise properties of antennas have only recently become a practical problem in communication systems, the subject of effective antenna noise temperature is an old one. An excellent derivation of the basic relationships was done by Burgess (Ref. 4) twenty years ago. A good discussion of the effect can be found in Ref. 5, together with World War II experimental data on antenna temperature measurements.

The basic fundamentals of antenna noise theory may be easily developed. It is well known that at a radio frequency, to an excellent approximation, the thermal noise generated by a matched load at T deg absolute (or Kelvin), is given by:

$$P = kT df \text{ watts} \quad (3)$$

where k is Boltzmann's constant of  $1.3803 \times 10^{-23}$  watt-sec/°K and df is the effective noise bandwidth. If we had a perfectly matched antenna with no dissipative losses, we would similarly discover that it had a noise output P due to reception of thermal noise from its environment. This noise may be defined in terms of an effective antenna noise temperature  $T_a$  as follows:

$$T_a \equiv \frac{P}{k df} \quad (4)$$

For an antenna with no dissipative or mismatch losses it can be shown (Ref. 5) through a straightforward derivation that effective antenna temperature will be given in spherical coordinates by:

$$T_a = \frac{1}{4\pi} \int_0^{2\pi} \int_0^\pi T(\theta, \phi) G(\theta, \phi) \sin \theta \, d\theta \, d\phi \quad (5)$$

where

$T(\theta, \phi)$  = black-body temperature of the antenna's environment

$G(\theta, \phi)$  = unnormalized antenna gain function

The practical feed design problem is somewhat obvious by reference to Fig. 2. A large dish is shown pointing at zenith, i. e., at 90-deg elevation. In order to achieve high aperture efficiency a feed might be used which strongly illuminates the outer region of the dish. Unfortunately, owing to the necessarily finite rate of angular cutoff of the feed radiation, the feed also significantly illuminates the ground. In accordance with the Reciprocity theorem, this also means that the antenna is susceptible to thermal noise radiation from the ground. As an example, if the ground had an effective noise temperature of 250°K, and the feed had a spillover of 10% in the angular region between the paraboloidal reflector edge and the horizon, Eq. (5) indicates a noise contribution of 25°K-- a serious effect on the performance of a low noise system. The effect of spillover on effective antenna temperature has been firmly established experimentally (Ref. 6).

A high-performance feed system should possess very low ground-directed spillover and, at the same time, high aperture efficiency.

### III. THE CASSEGRAINIAN SYSTEM

An excellent article on the Cassegrainian system has been recently published (Ref. 7). The basic geometry of the system can be seen in Fig. 3. A hyperboloidal subreflector is interposed between the focal point of the reflector and the reflector surface. The hyperbola is chosen as the curve for the subreflector in order to achieve the desired constant path length and correct ray direction. It can be seen from simple ray-tracing that, based on geometrical optics, the Cassegrainian system has no spillover. In practice, however, the subreflector is only moderately sized in terms of a wavelength and hence the geometrical optics approximation breaks down.

The approximate effect of the subreflector wavelength size on spillover and edge taper may be derived from simple considerations. In Fig. 4 a hyperboloidal subreflector is shown, together with a conical approximation. The latter is formed by approximating the hyperbola by a series of tangential straight-line segments. The resulting curve is then revolved about its axis of symmetry to generate the hypothetical subreflector surface. The scattering pattern of each conical ring may be added to derive the total subreflector scattering pattern. This technique is certainly rigorous in the limit of zero ring width (i. e., a true hyperboloid). Unfortunately, the computational problem becomes difficult in this limit, and the solution yields little or no physical insight into the problem of modifying the surface to enhance performance.

Since each ring is essentially uniformly illuminated, each ring scatters an approximately  $\sin X/X$  type of radiation pattern, whose maximum will be in

the direction indicated by geometric ray-tracing. To verify this experimentally, a conical ring was constructed and its scattering pattern measured. The geometry of the ring scatterer is shown in Fig. 5. The measured scattering pattern is shown in Fig. 6. As can be seen in this pattern, the peak radiation occurs almost exactly at the optically predicted angle of 57 deg. The half-power beam-width predicted by the  $\sin X/X$  pattern for a ring of this width is 28 deg, excellent agreement with the measured value of 30 deg shown in Fig. 6.

The largest-width ring which may be used in the hypothetical conical ring model of the hyperboloidal subreflector is that size which will introduce negligible pattern ripple when the individual ring-scattering patterns are added together. This point will occur when the scattering patterns overlap at roughly their 6-db points.

A sample calculation is shown in Fig. 7. In this example an 8-wavelength-diameter subreflector is approximated by two cones, the central, truncated cone being 4 wavelengths in diameter and the outer, angular cone being 2 wavelengths wide on each side. In Fig. 8 the predicted pattern is shown on a logarithmic scale. A resemblance to Fig. 6 can be seen.

#### IV. BEAMSHAPING MODIFICATION

From the qualitative analysis presented in the preceding section, one would intuitively expect that a conical flange at the outer edge of a hyperboloidal subreflector could control spillover radiation. The conical extension flange was used to develop a high quality, 960-mc, Cassegrainian shaped-beam feed system for an 85-ft paraboloidal antenna. The application for the system required not

only high aperture efficiency but also an extremely low effective antenna noise temperature. In order expeditiously to derive a near-optimum design without extensive full-scale testing, extensive 1/10-scale tests were performed on the feed system. Figure 9 shows the geometry of the flange modification. Figure 10 is a photograph of the feed system on the specially constructed foam mount that was used for pattern tests. Figure 11 is a close-up photograph of the modified subreflector. The conical vertex plate in the center is used for impedance matching purposes (Ref. 8).

A series of different flange configurations was experimentally evaluated. In all cases, the hyperboloid had a diameter of 9.6 in. (approximately 8 wavelengths) and a half-aperture angle of 60 deg. Also, a uniform flange diameter of 14 in. was used. Complete data were taken for flange angles of 15.4, 18.4, 21.4, and 24.4 deg. The latter case corresponds to a tangential extension of the hyperboloid. Figures 12, 13, 14, and 15 show the E- and H-plane patterns for, respectively, the 15.4-, 18.4-, 21.4-, and 24.4-deg cases. Diagonal (45-deg) plane patterns and diagonal plane cross-polarized patterns were also taken for each case. As an example, Fig. 16 and 17 show, respectively, the 45-deg-plane and cross-polarized 45-deg patterns for the 18.4-deg case.

The radiation patterns obtained within the unmodified subreflector are shown in Fig. 18 through 21. It can be seen from comparison with Fig. 12 through 17 that the beamshaping flange effects a drastic improvement in the spillover performance. The radiation patterns were graphically integrated to determine spillover in various angular regions. The result is shown in Fig. 22 as a function of the flange angle.

The phase front properties of the modified subreflector were measured with the Serrodyne system (Ref. 9) shown in Fig. 23. A typical plot of the measured phase front deviation is shown in Fig. 24. Both the flange and the vertex plate contribute to the phase error.

The expression given in Section II for calculating aperture efficiency (Eq. 2) assumes a uniformly phased aperture. The integral in this expression may, however, be broken down into the sum of a number of differently phased integrals which may be added vectorially. An example will clarify this technique. In Fig. 25 the pattern that was shown in Fig. 16 is replotted on specially constructed paper whose abscissa has been weighted to include the  $\tan(\psi/2)$  factor in Eq. (2). Thus, on this type of paper (Ref. 3), the area under the curve is directly proportional to the aperture integral. The area under the curve may be then divided into adjacent vertical strips, each of which is reasonably constant in phase. The aperture may thus be represented as the sum of a series of small vectors whose magnitudes are given by the strip areas and whose arguments are given by a phase plot such as Fig. 24. The vector addition process is shown in Fig. 26. From (2) the phase error efficiency loss is given by the square of the ratio of the resultant vector to the sum of its component vectors. In this example, the phase error loss is approximately 0.5 db.

One last factor--the feed system gain--must be determined before (2) may be used to estimate the aperture efficiency which will be achieved with a feed system. In the feed system described here, two methods were used: the directivity was calculated by feed system pattern integration, and the gain was

measured by the standard horn substitution method. The results of these two methods are shown in Table 1.

Table 1. Comparison of feed system gain measurement and pattern integration

Flange angle deg	Measured gain db	Calculated directivity db	Discrepancy db
15.4	9.25	9.04	+0.21
18.4	8.47	8.51	-0.04
21.4	8.46	8.54	-0.08
24.4	8.89	8.72	+0.17

It was concluded that use of the calculated directivity rather than the measured gain would yield more consistent results. The calculated aperture efficiency corresponding to the modified subreflector is shown in Fig. 27 as a function of flange angle.

## V. FULL-SCALE TESTS

After successful completion of the scale-model tests, a full-scale modified Cassegrainian system was designed, installed, and tested in the 85-ft Goldstone polar-mount antenna. Based on Fig. 27, the 18.4-deg flange angle was chosen as being a suitable compromise between aperture efficiency and low noise performance. A photograph of the completed installation is shown in Fig. 28.

Extensive pattern, gain, and noise temperature tests were performed on the installation in an attempt to correlate full-scale performance to that predicted

from the scale-model tests. In general, excellent agreement was observed. The measured aperture efficiency was  $50\% \pm 8\%$ , while that predicted by Fig. 27 is  $58\%$ . The measured zenith noise temperature was  $9.5^\circ\text{K} \pm 2^\circ\text{K}$ , which may be predicted as follows:

Galactic background, atmospheric loss, extragalactic background (measured)	3.5°K
1.3% spillover (from scale-model tests, Fig. 22)	3
1% scattering from the quadripod support structure	3
Total	<u>9.5°K</u>

Full-scale pattern tests were performed in a further attempt to relate primary to secondary performance. This relationship is particularly pertinent in a Cassegrainian system which has the additional effects of subreflector blockage and forward spillover, neither of which exists in conventional focal point systems. Figures 29 and 30 show, respectively, the E- and H-plane measured secondary patterns, together with the predicted wide-angle sidelobe envelope based on the feed system measured characteristics. The prediction does not include spurious radiation due to the quadripod support structure. As can be seen from Fig. 29 and 30, the general agreement between the primary pattern characteristics and the secondary patterns is qualitatively good.

## ACKNOWLEDGMENT

The full-scale Cassegrainian system was the result of the efforts of many Jet Propulsion Laboratory personnel. The feed horn electrical design was done by Danver Schuster and the transmission line components by Gerald Levy. The noise temperature measurement instrumentation was designed by Charles Stelzried. The entire structural and mechanical design for the full-scale installation was done by M. Smoot Katow. Finally, the author wishes to thank William D. Merrick and Robertson Stevens for their enthusiastic support of the project.

## REFERENCES

1. Potter, P. D., Cassegrainian Subreflector Flange, Invention Report No. 30-92, Jet Propulsion Laboratory, Pasadena, Calif., October 12, 1961.
2. Silver, S., Microwave Antenna Theory and Design, Vol. 12, Radiation Laboratory Series, Massachusetts Institute of Technology, McGraw-Hill Book Co., 1949.
3. Potter, P. D., The Aperture Efficiency of Large Paraboloidal Antennas as a Function of Their Feed System Radiation Characteristics, Technical Report No. 32-149, Jet Propulsion Laboratory, Pasadena, Calif., October, 1961.
4. Burgess, R. E., "Noise in Receiving Aerial Systems," Proceedings of the Physical Society, London, Vol. 53, pp. 293-304, 1941.
5. Lawson, J. L., and G. E. Uhlenbeck, Threshold Signals, Vol. 24, Radiation Laboratory Series, Massachusetts Institute of Technology, McGraw-Hill Book Co., 1950.
6. Schuster, D., C. T. Stelzried, and G. S. Levy, The Determination of Noise Temperatures of Large Antennas, Technical Report No. 32-97, Jet Propulsion Laboratory, Pasadena, Calif., May 1, 1961.
7. Hannon, P. W., "Microwave Antennas Derived from the Cassegrain Telescope," IRE Transactions on Antennas and Propagation, Vol. AP-9, No. 2, pp. 140-153, March 1961.
8. Foldes, P., and S. Komlos, "Theoretical and Experimental Study of Wide Band Paraboloid Antenna with Central Reflector Feed," RCA Review, Vol. XXI, No. 1, pp. 94-116, March 1960.
9. Cumming, R. C., "The Servodyne Frequency Translator", Proceedings of the IRE, Vol. 45, pp. 175-186, February 1957.

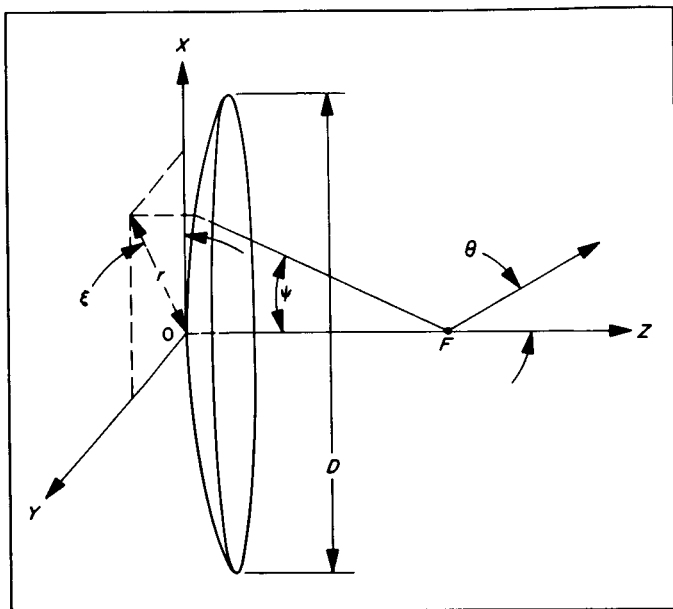
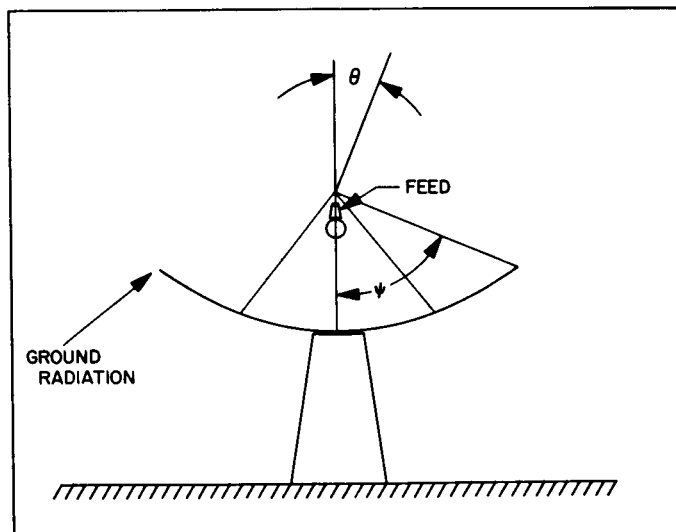


Fig. 1. Paraboloid geometry

Fig. 2. Effect of spillover



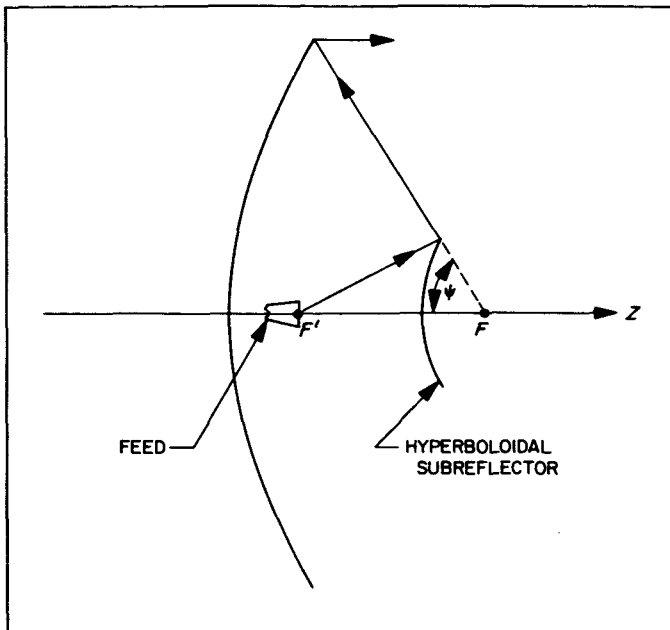
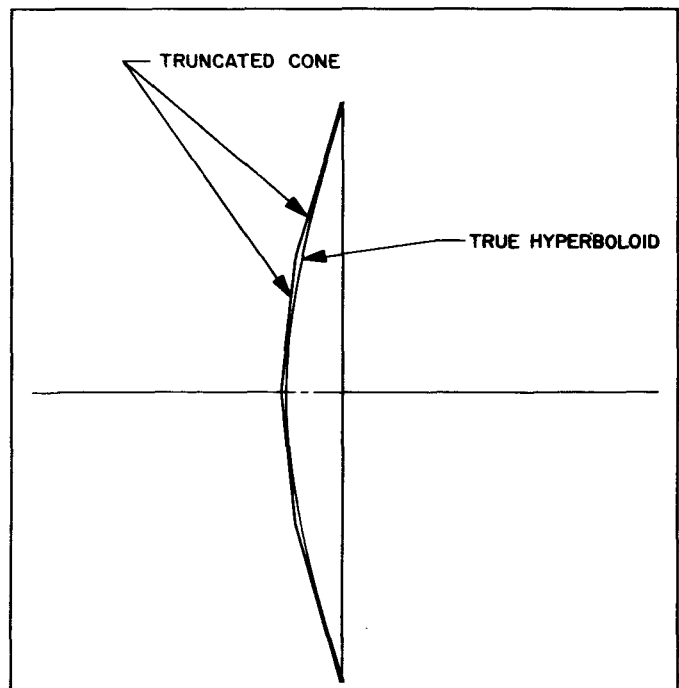


Fig. 3. Cassegrainian system

Fig. 4. Conical subreflector approximation



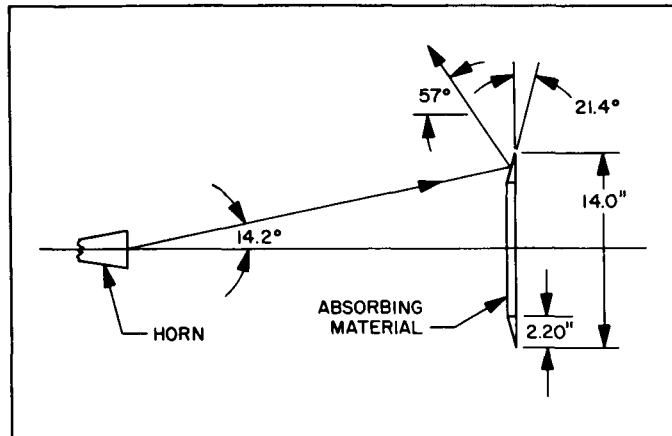


Fig. 5. Experimental ring scatterer



Fig. 6. Measured scattering pattern of ring

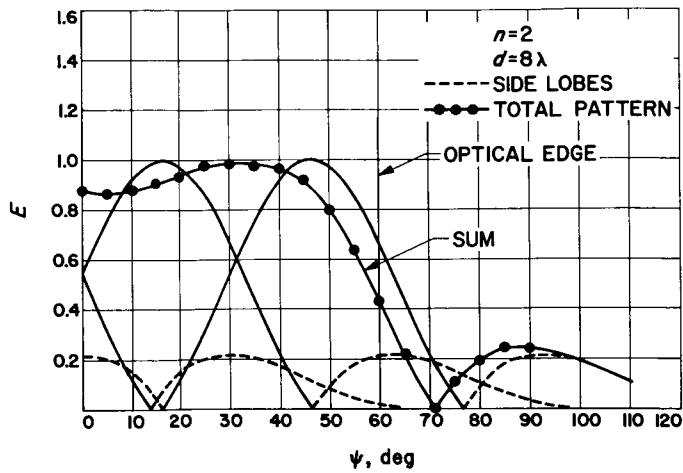


Fig. 7. Cassegrainian pattern synthesis

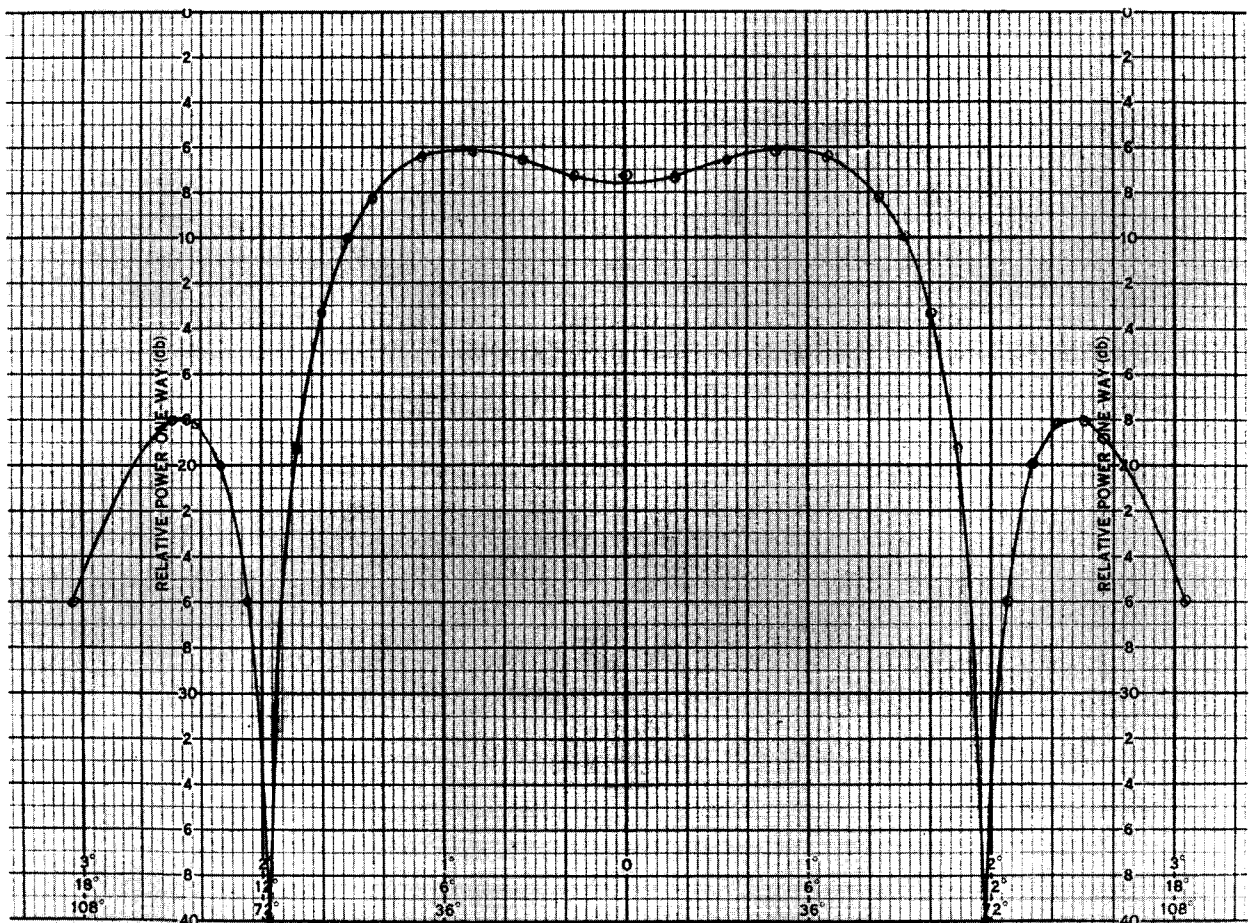


Fig. 8. Predicted Cassegrainian pattern

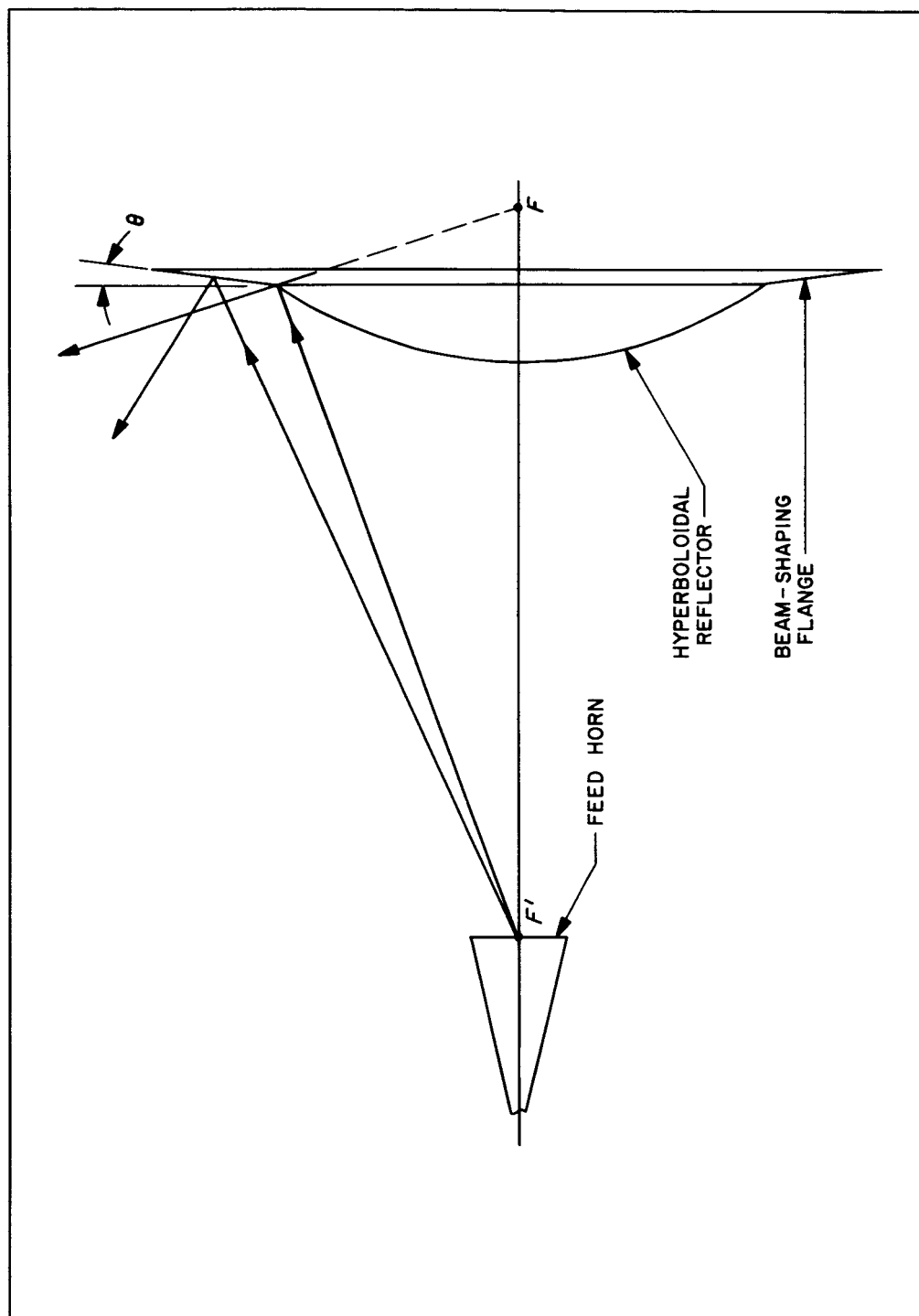


Fig. 9. Geometry of shaped-beam subreflector

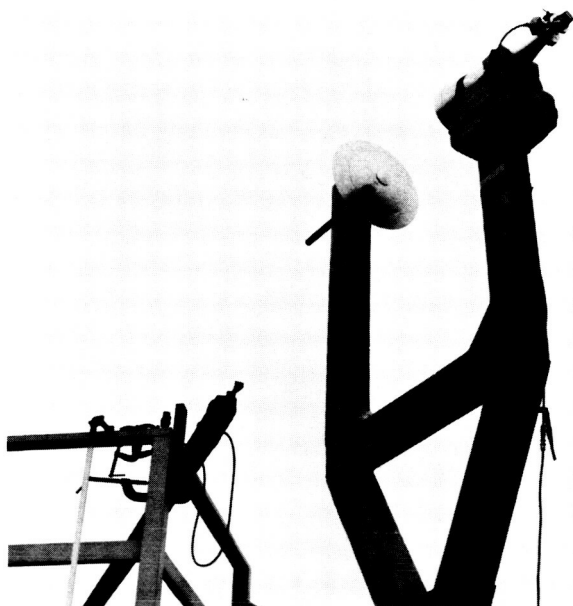


Fig. 10. Scale model feed system and mount



Fig. 11. Scale model subreflector

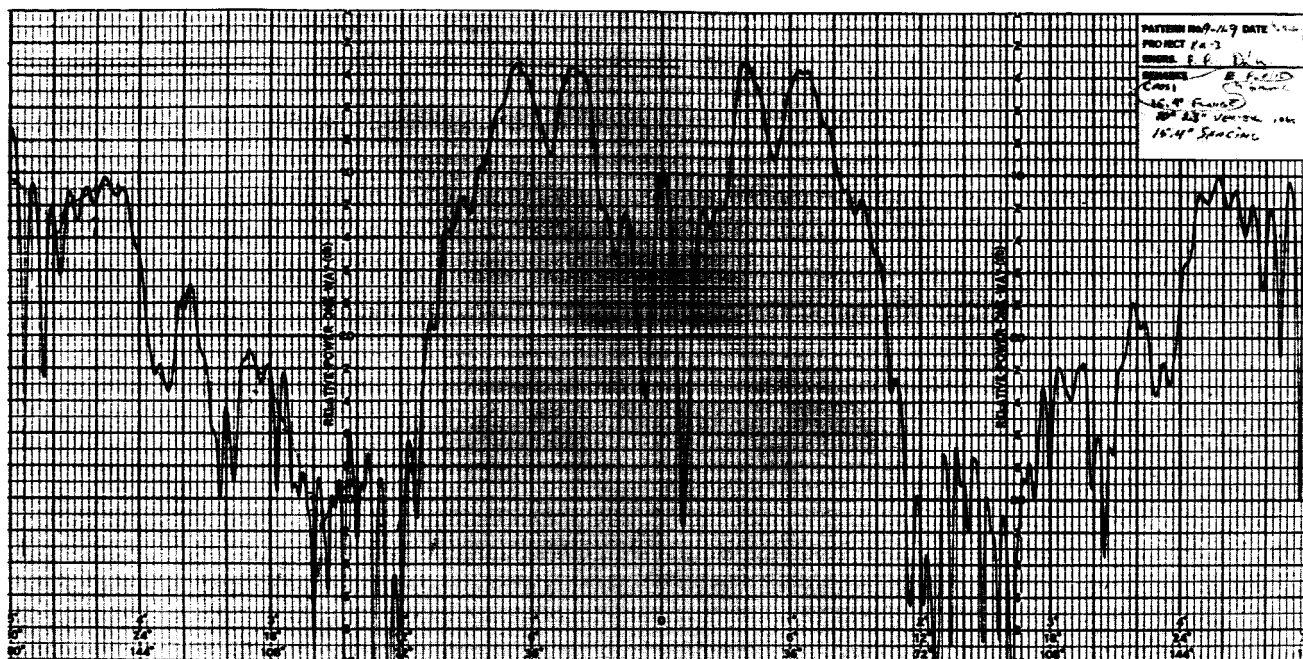


Fig. 12a. E-plane pattern of modified reflector,  $\theta = 15.4$  deg

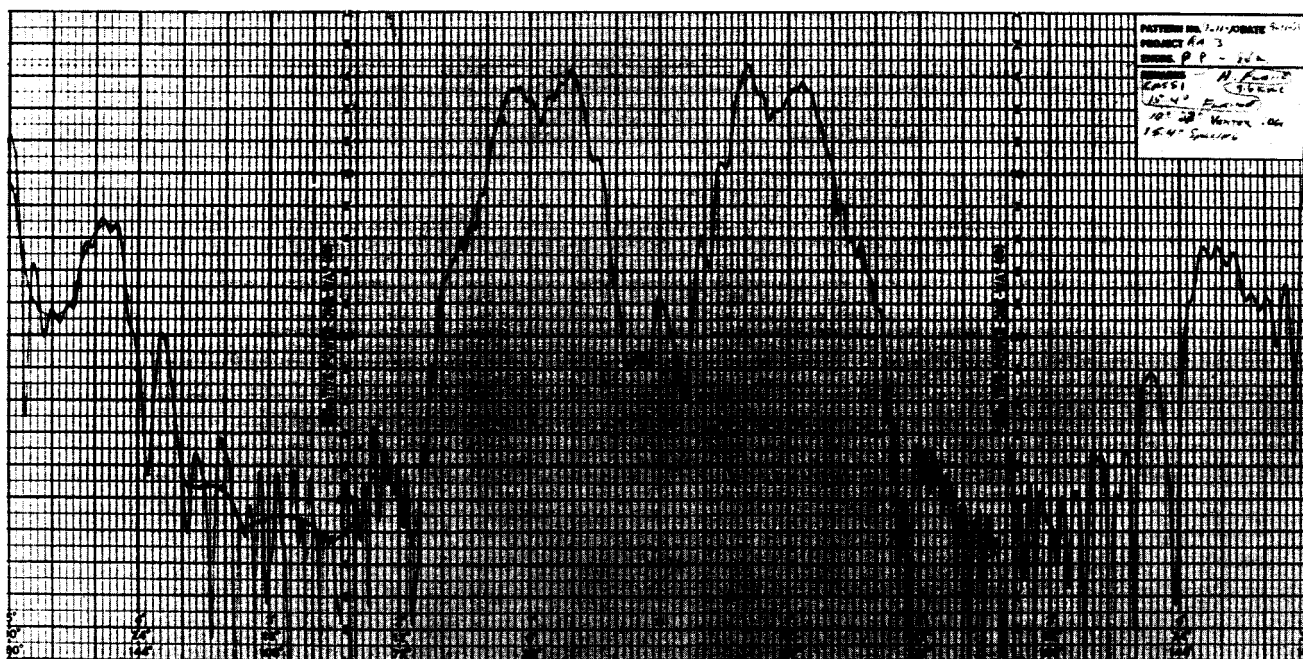
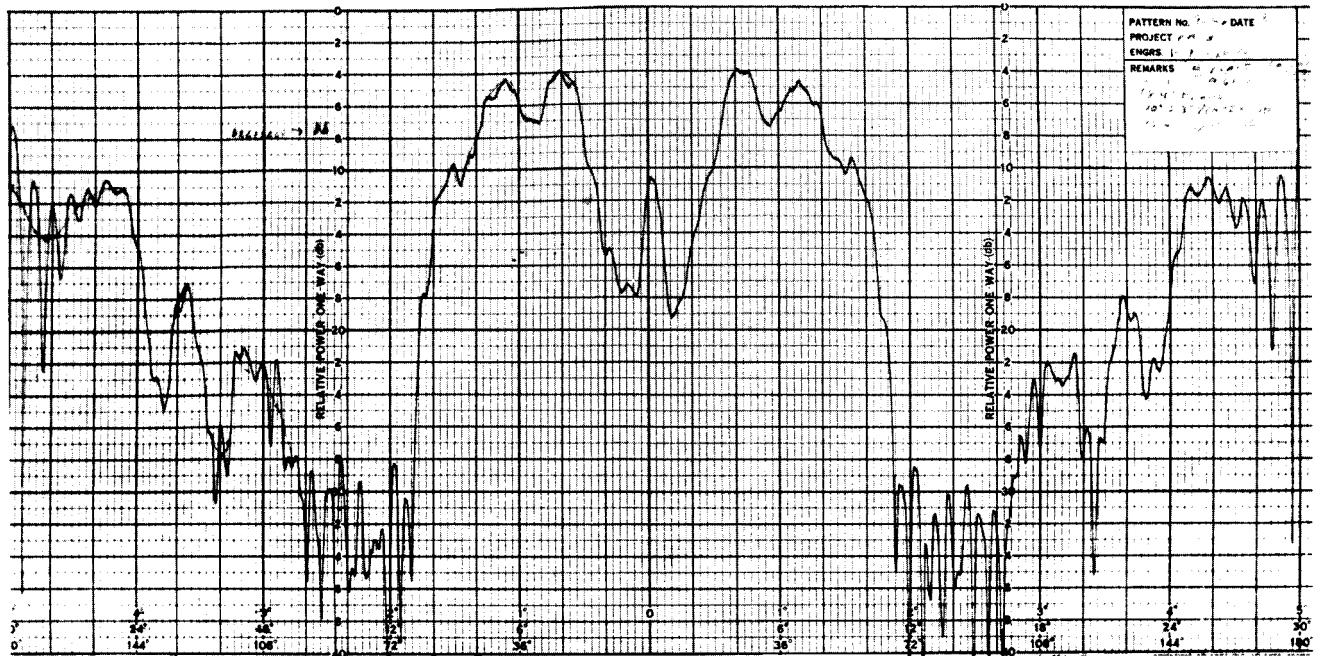
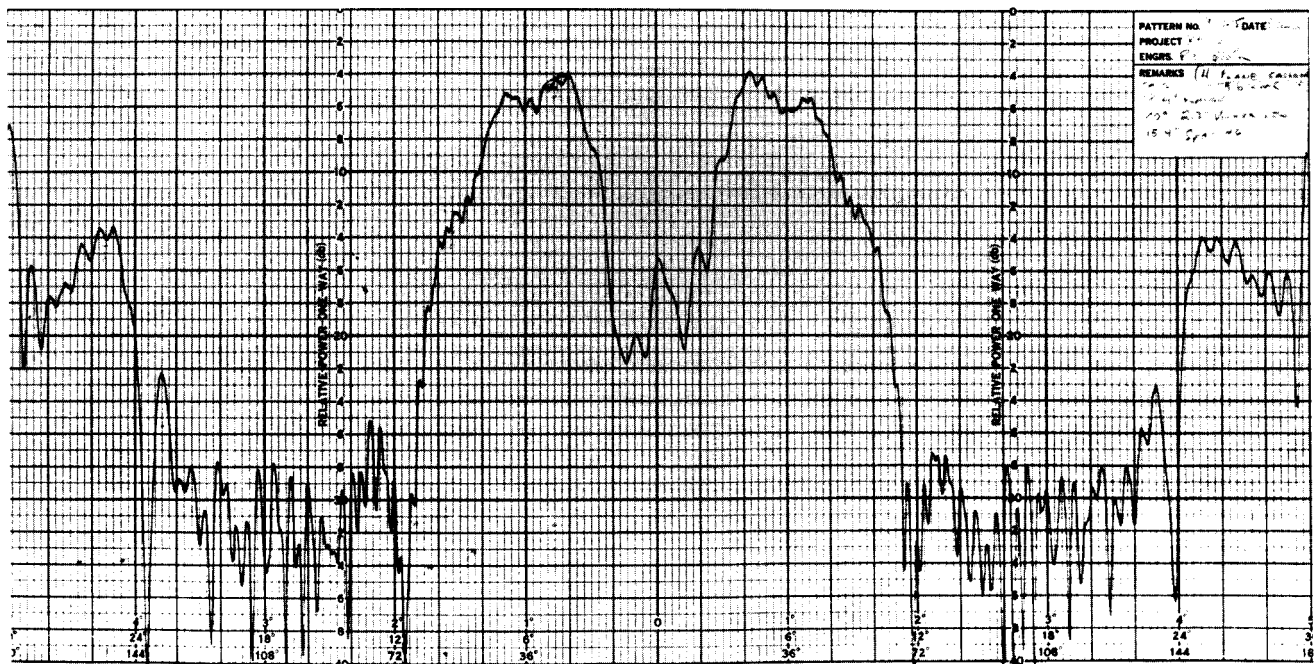
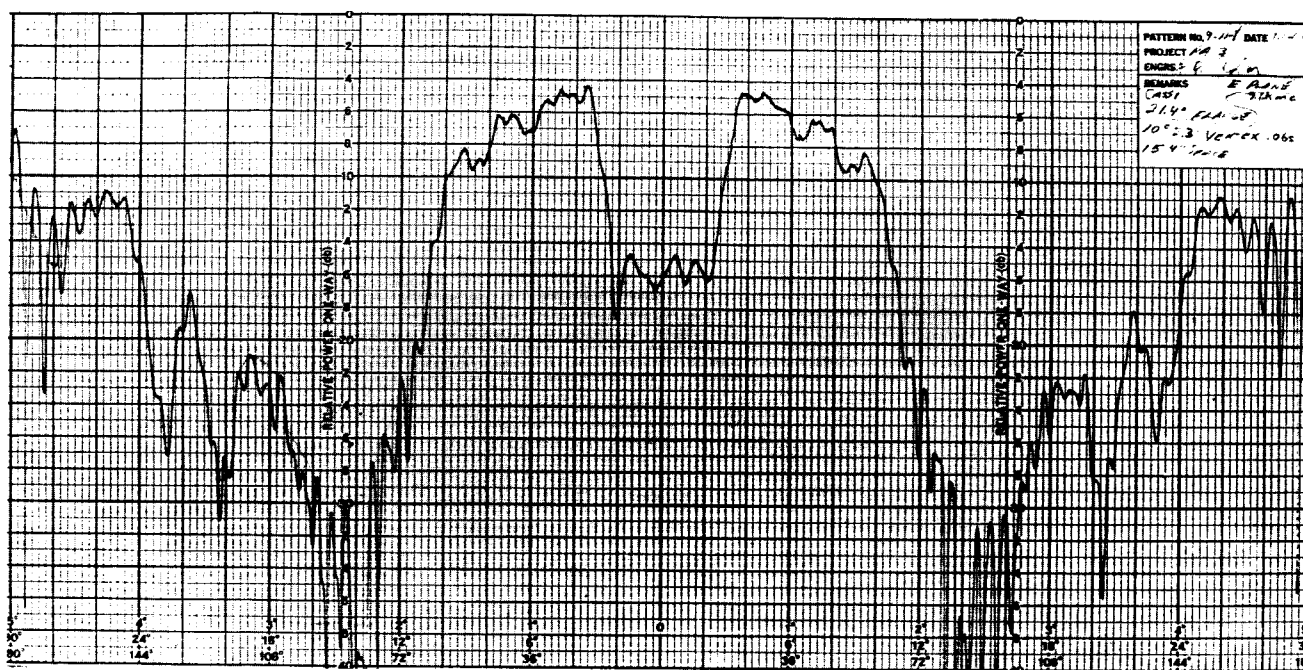
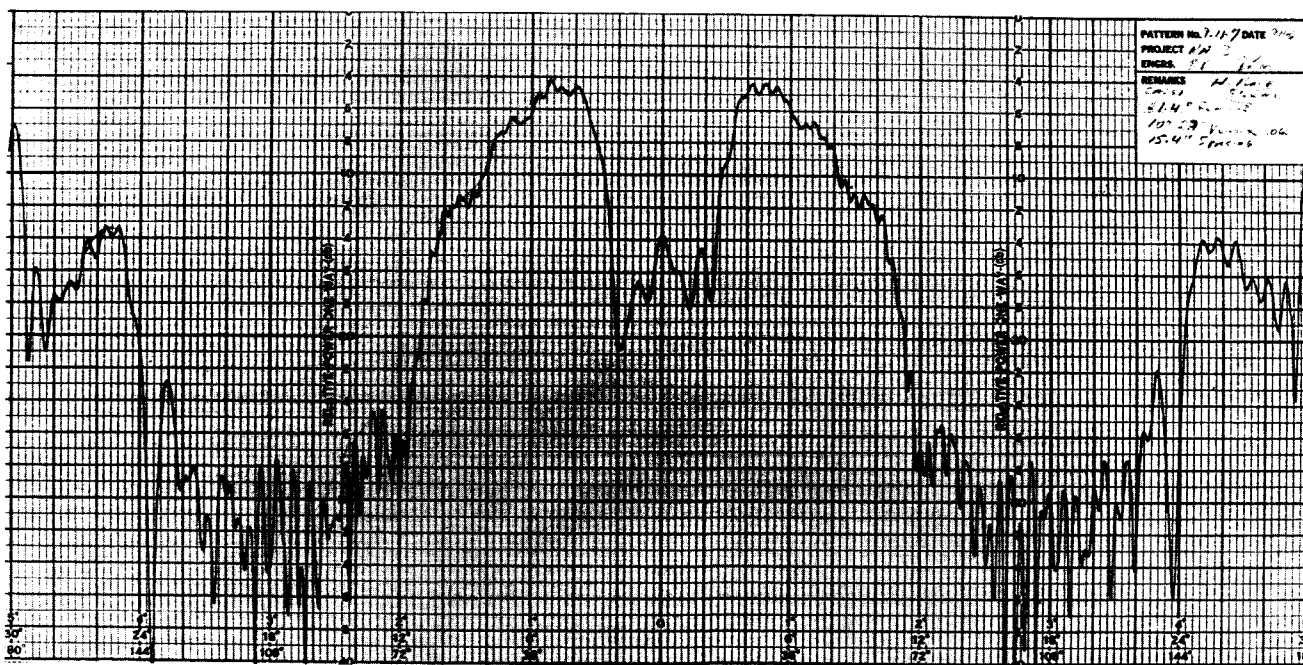


Fig. 12b. H-plane pattern of modified reflector,  $\theta = 15.4$  deg

Fig. 13a. E-plane pattern of modified reflector,  $\theta = 18.4$  degFig. 13b. H-plane pattern of modified reflector,  $\theta = 18.4$  deg

Fig. 14a. E-plane pattern of modified reflector,  $\theta = 21.4$  degFig. 14b. H-plane pattern of modified reflector,  $\theta = 21.4$  deg

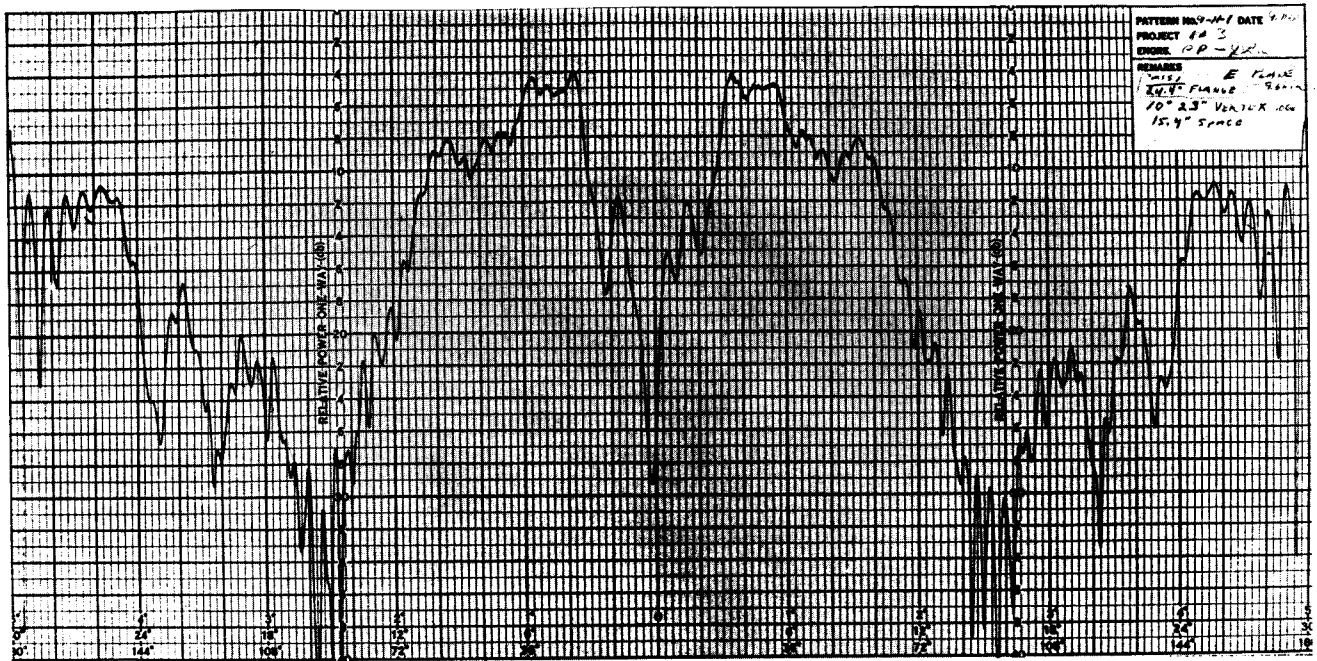


Fig. 15a. E-plane pattern of modified reflector,  $\theta = 24.4$  deg

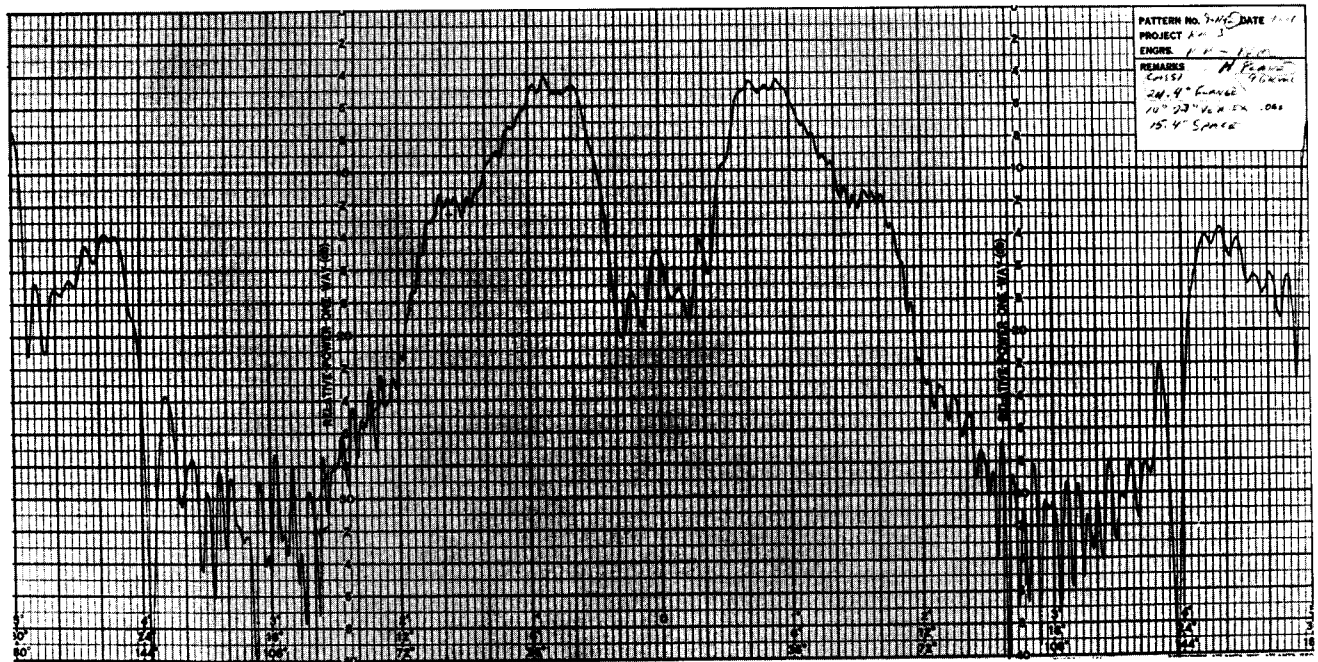


Fig. 15b. H-plane pattern of modified reflector,  $\theta = 24.4$  deg

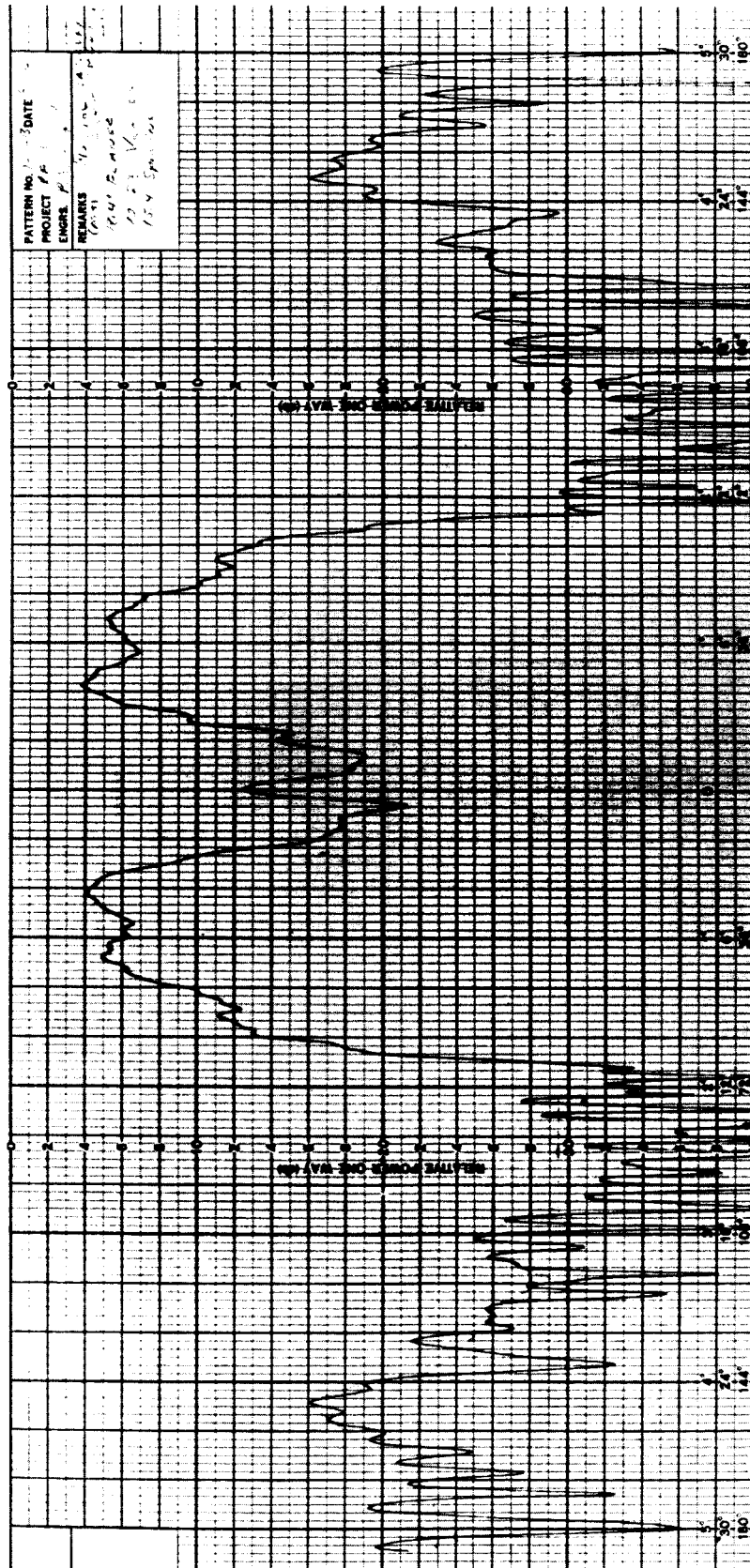


Fig. 16. 45-deg-plane pattern of modified subreflector,  $\theta = 18.4$  deg

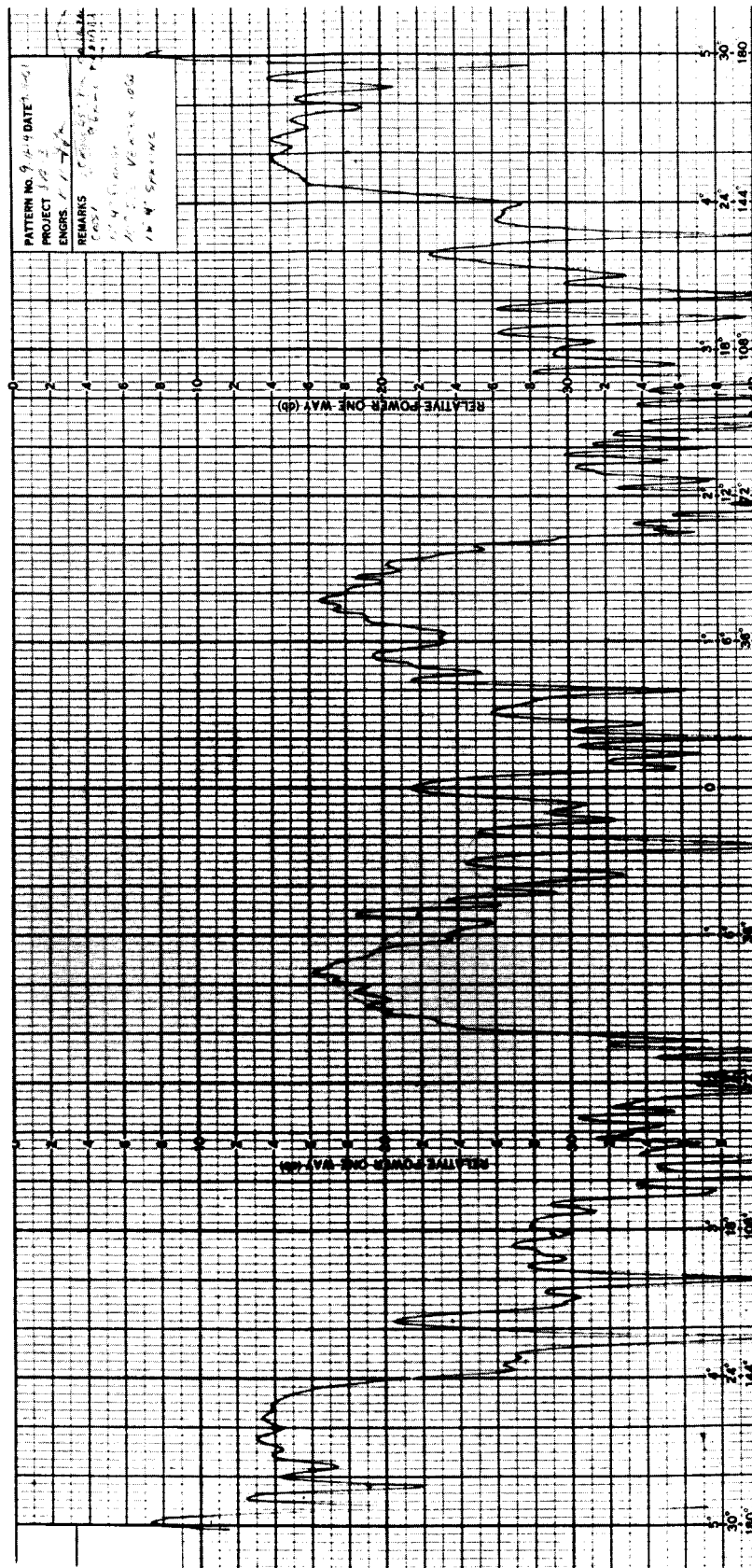


Fig. 17. \_ Cross-polarized 45-deg-plane pattern of modified subreflector,  $\theta = 18.4$  deg

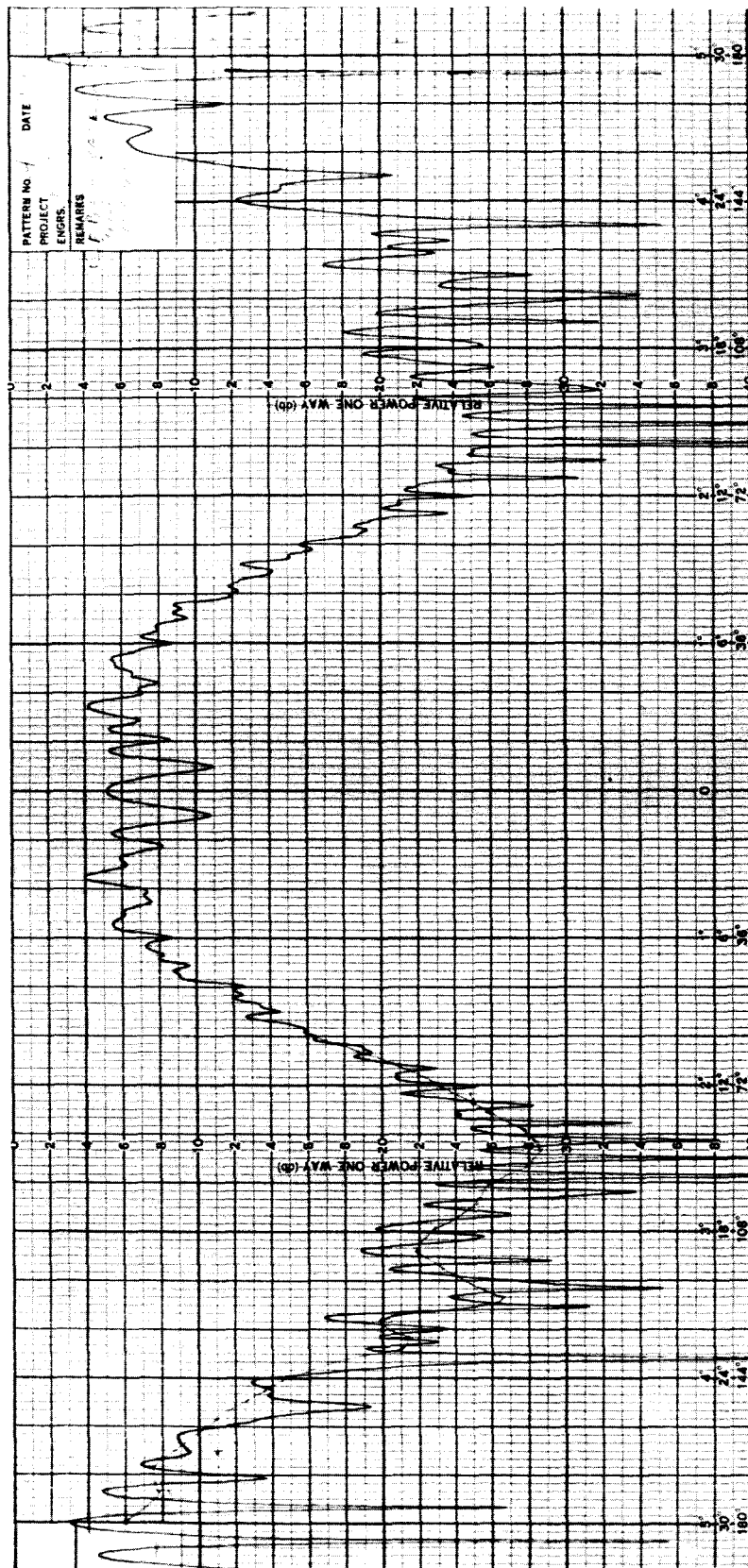


Fig. 18. E-plane pattern of unmodified subreflector

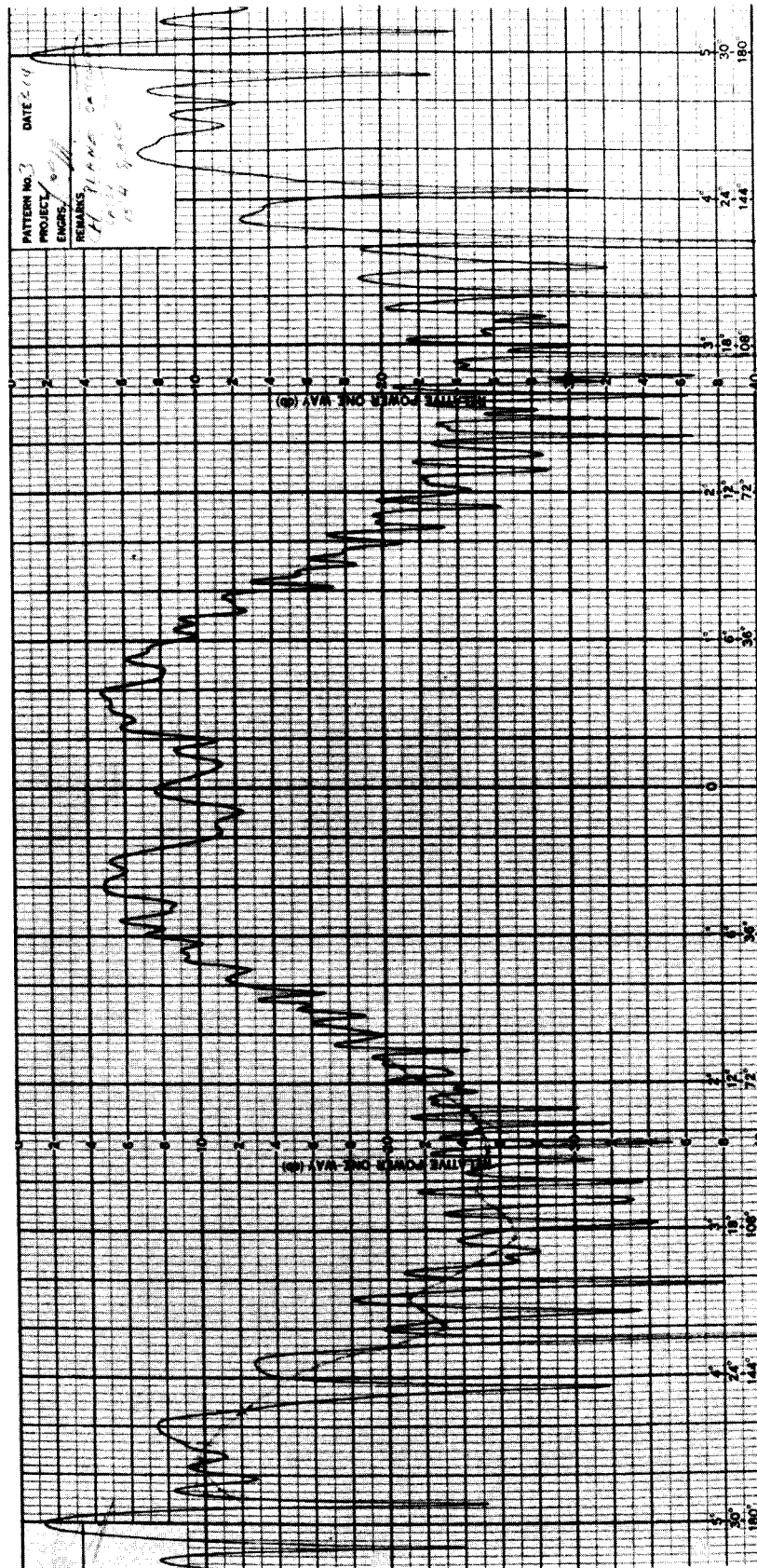


Fig. 19. H-plane pattern of unmodified subreflector

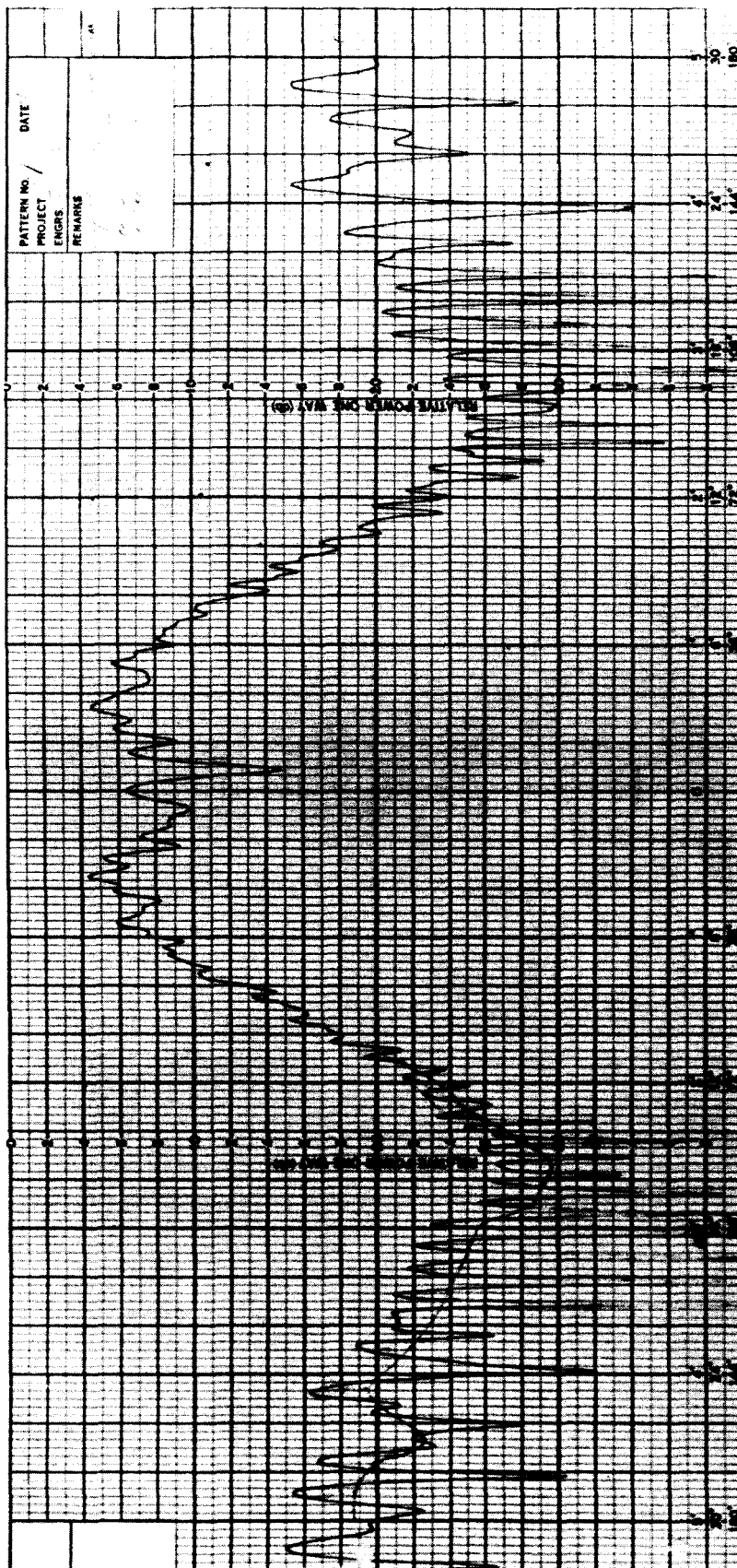


Fig. 20. 45-deg-plane pattern of unmodified subreflector

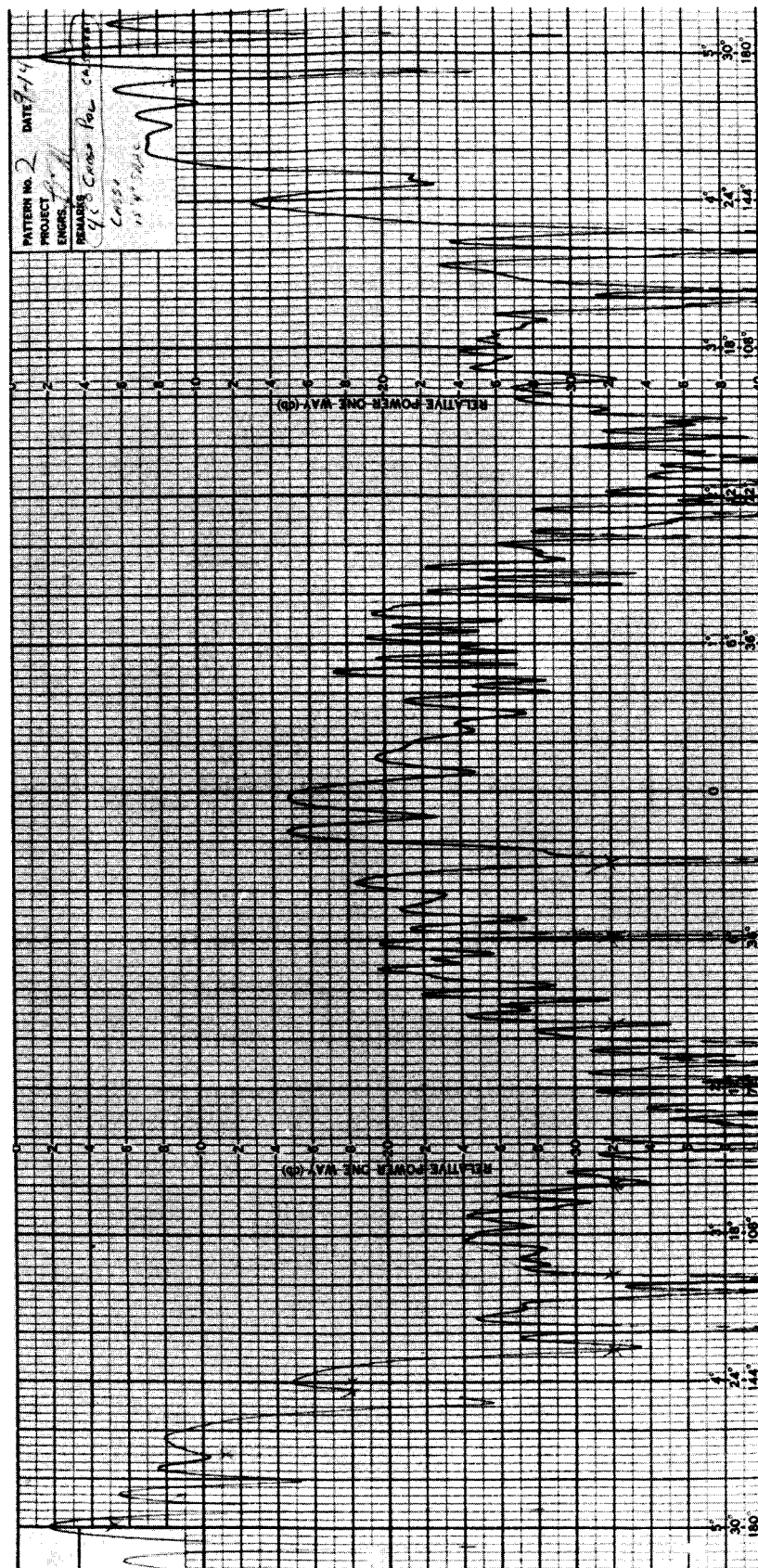


Fig. 21. Cross-polarized 45-deg-plane pattern of unmodified subreflector

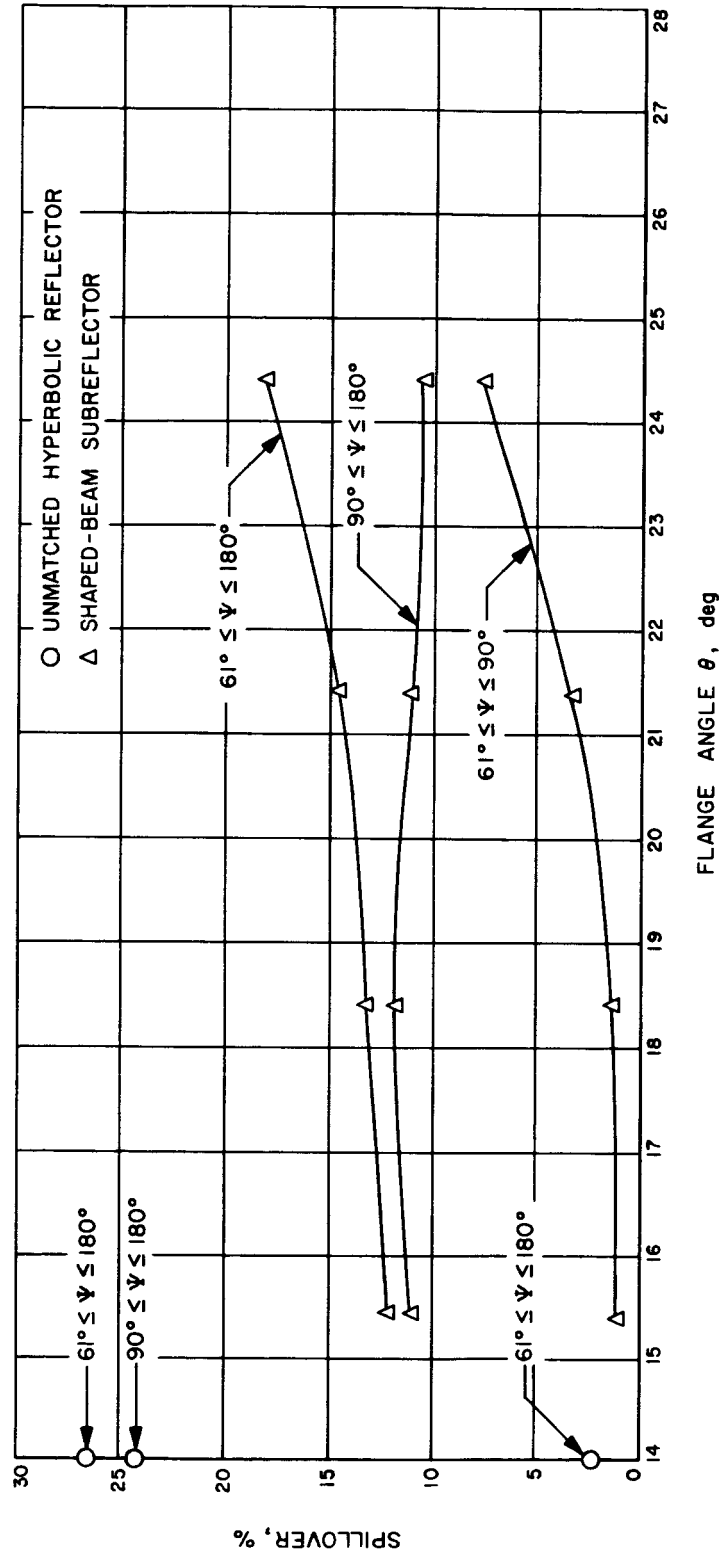


Fig. 22. Spillover vs flange angle

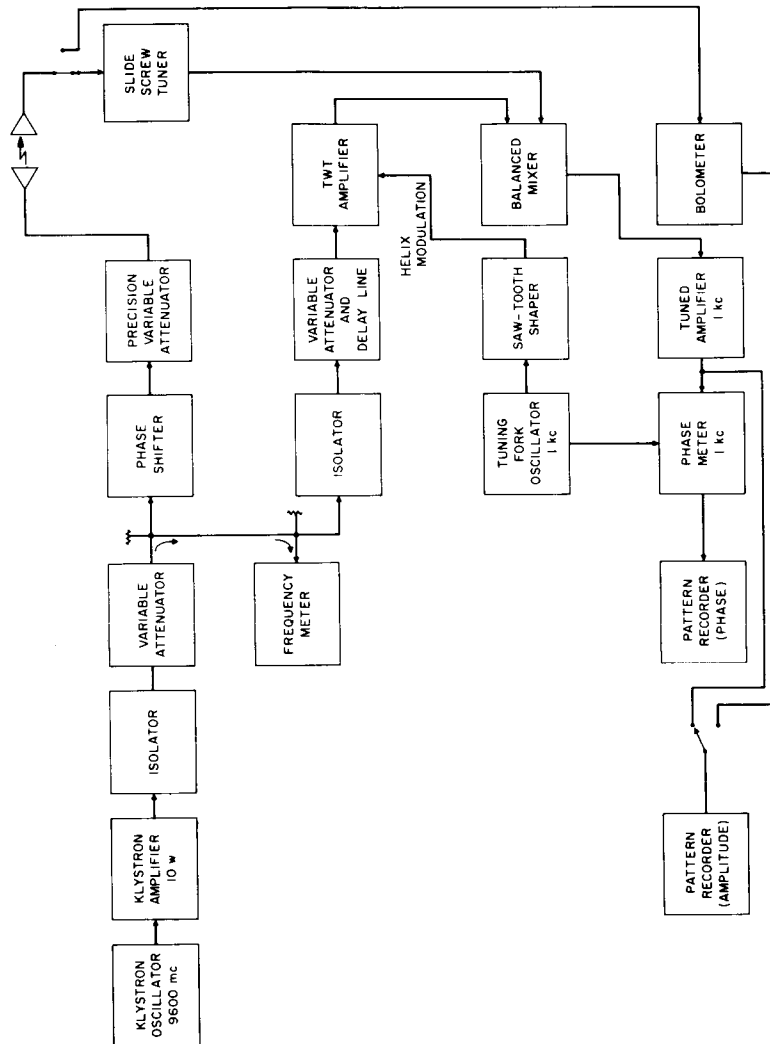


Fig. 23. Phase measuring system

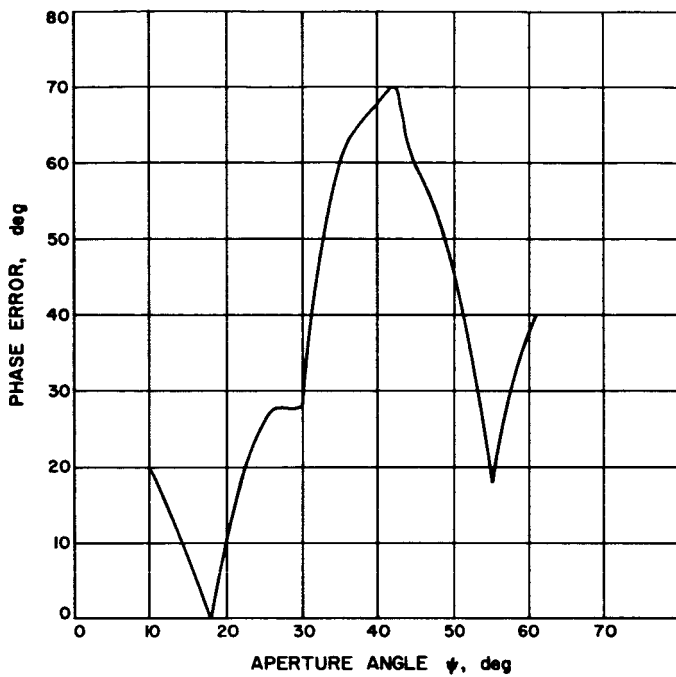


Fig. 24. Phase error plot, 45-deg plane,  $\theta = 18.4$  deg

Fig. 25. Aperture integration plot, 45-deg plane,  $\theta = 18.4$  deg



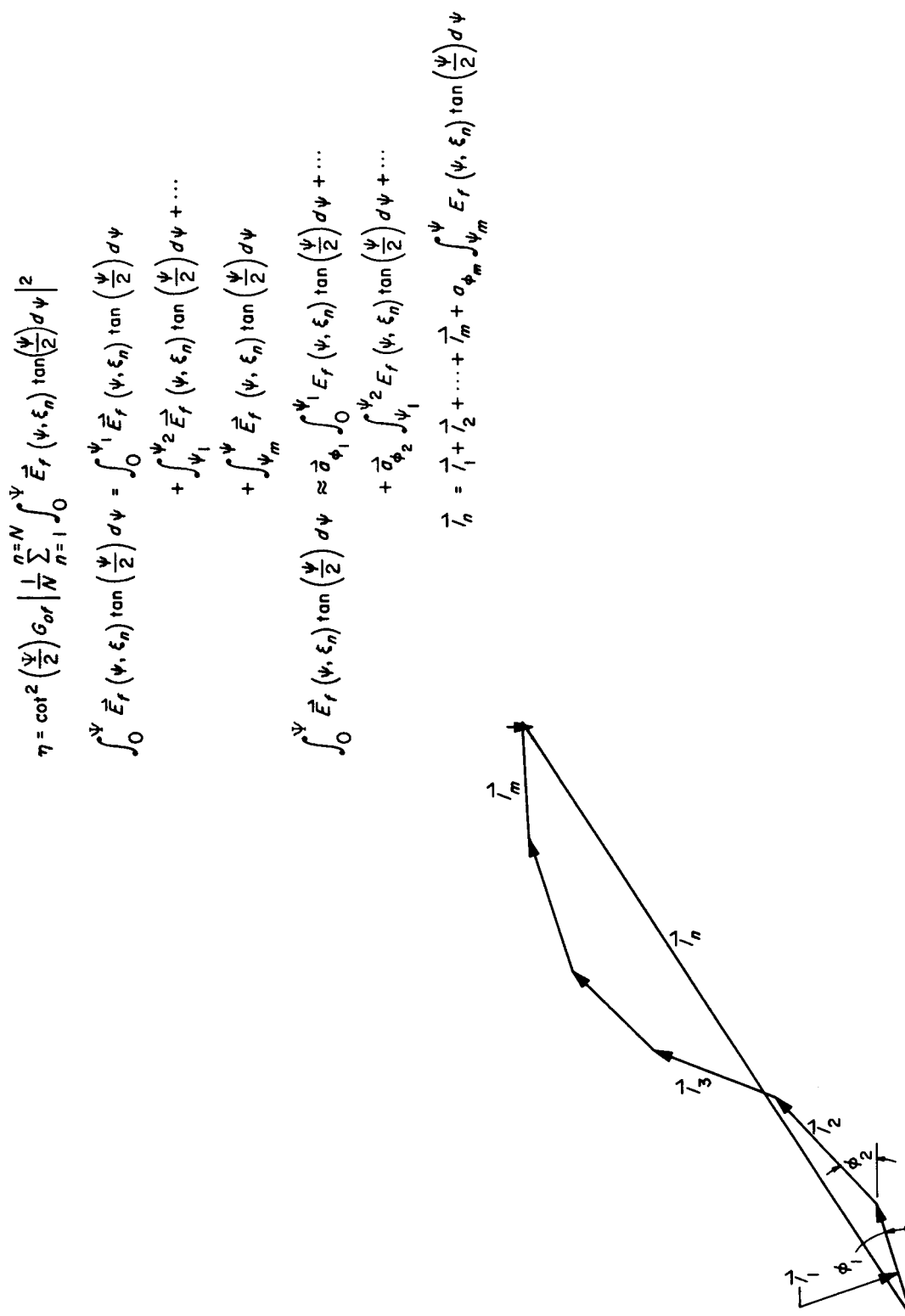


Fig. 26. Vector integration diagram

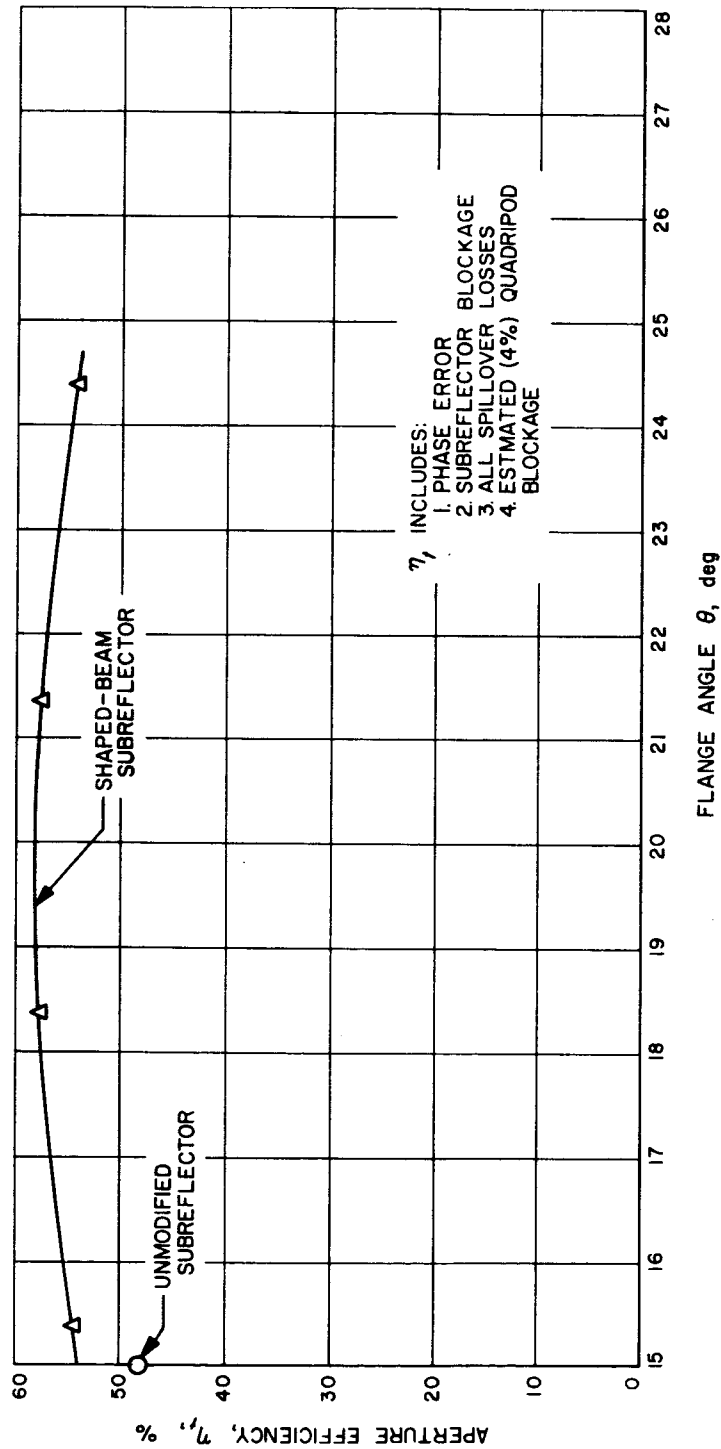


Fig. 27. Aperture efficiency vs flange angle

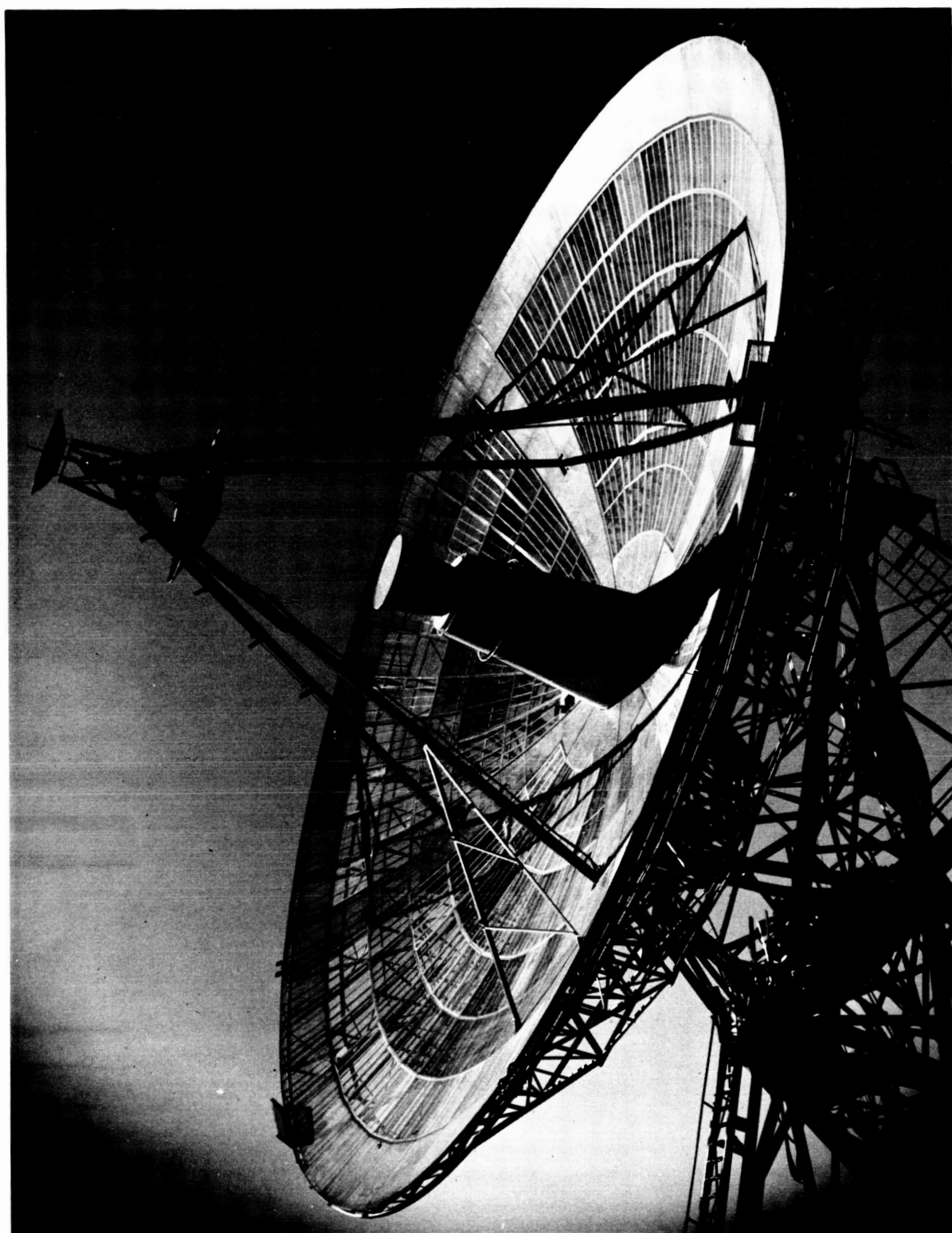


Fig. 28. Full-scale Cassegrainian installation

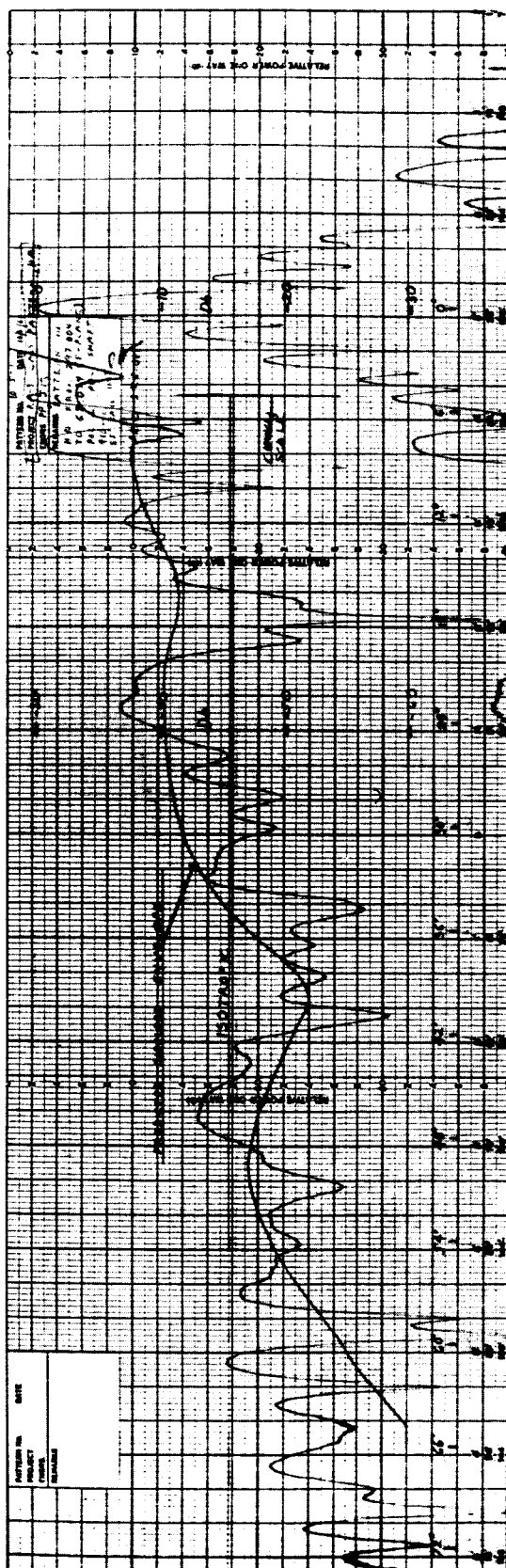


Fig. 29. Secondary pattern, E-plane

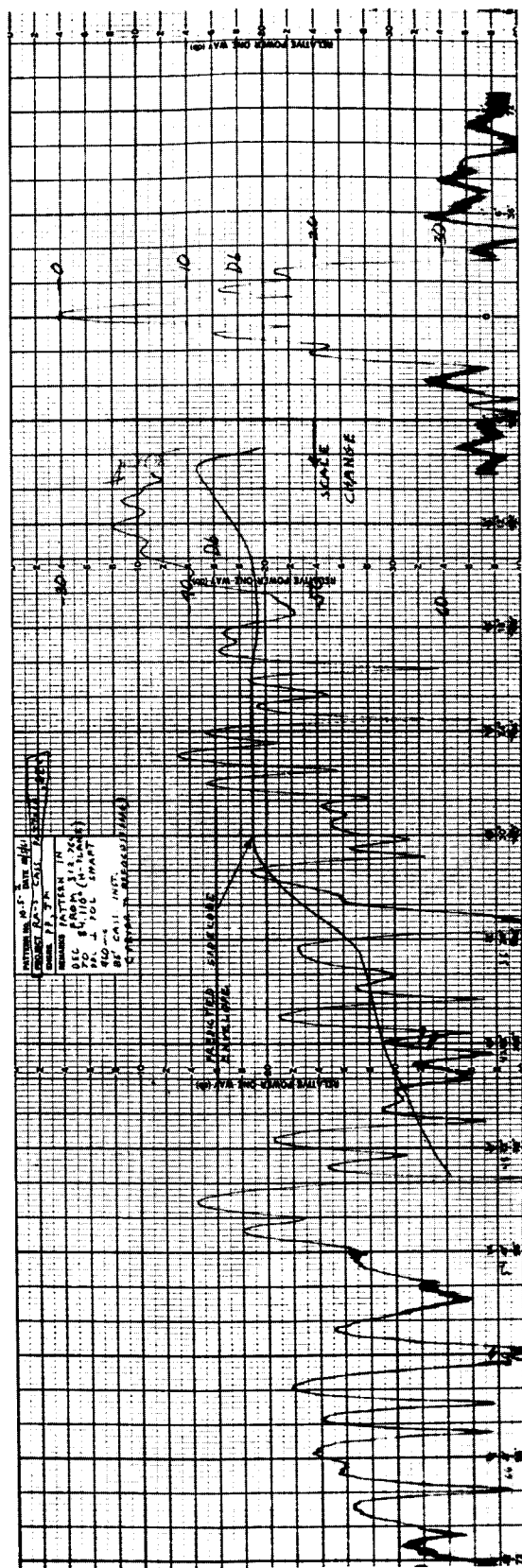


Fig. 30. Secondary pattern, H-plane